Nano Energy 70 (2020) 104504

Contents lists available at ScienceDirect

Nano Energy

journal homepage: http://www.elsevier.com/locate/nanoen

Full paper

$Li_{4.4}Sn$ encapsulated in hollow graphene spheres for stable Li metal anodes without dendrite formation for long cycle-life of lithium batteries

Yong Jiang [a], Jinlong Jiang [a], Zhixuan Wang [a], Mingrui Han [a], Xiaoyu Liu [b], Jin Yi [b], Bing Zhao [a,b,**], Xueliang Sun [b], Jiujun Zhang [b,*]

[a] School of Environmental and Chemical Engineering, Shanghai University, Shanghai, 200444, China
[b] Institute for Sustainable Energy/College of Science, Shanghai University, Shanghai, 200444, China

ARTICLE INFO

Keywords:
Closed hollow graphene sphere
Lithiophilic $Li_{4.4}Sn$
Tip effect
Uniform Li nucleation
Li metal anodes
Dendrite formation

ABSTRACT

Lithium (Li) metal has always faced serious challenges of dendritic growth and low Coulombic efficiency due to the nonuniform electric field distribution and the dynamically changed interface situation. In this paper, the interconnected and closed hollow graphene spheres with an internal load of lithiophilic $Li_{4.4}Sn$ nanoparticles ($Li_{4.4}Sn$/SG) is prepared to improve Li deposition behavior. Both the density functional theory calculations and experimental studies indicate that $Li_{4.4}Sn$ has higher binding energy and lower nucleation overpotential toward Li than graphene, thus guiding the deposition of Li metal inside the hollow graphene spheres to avoid the generation of uncontrolled Li dendrites and formation of solid electrolyte interface (SEI) on the fresh Li surface. Furthermore, the surface of the non-tip graphene spheres can greatly avoid the uneven distribution of charge caused by the tip effect, so as to continuously guide the uniform deposition of Li on the surface of the spheres after the spheres are completely filled with Li, thus achieving a dense Li metal layer free of dendrites. In consequence, the $Li_{4.4}Sn$/SG electrode exhibits a long lifespan up to 1000 h and an exceptionally low overpotential (<18 mV). It is believed that the design of the closed hollow spherical structure with lithiophilic nanoparticle seeds inside is a promising strategy to construct high performance Li metal anodes for lithium batteries.

1. Introduction

In recent years, lithium batteries with high energy/power densities have been becoming one kind of the most important and practical batteries for many applications including portable electronics, electric vehicles, and grid storage [1,2]. This is because Li metal has a high theoretical capacity of 3860 mA h g^{-1} and a low negative electrochemical potential of −3.04 V (vs the standard hydrogen electrode) [3–6]. However, the application of Li metal anodes is facing some challenges, especially the deposition of Li metal tends to generate Li dendrite. When a Li battery undergoes charge/discharge cycling, the formed dendritic Li can break to form dead Li, resulting in a new solid electrolyte interface (SEI) layer. This SEI layer could leading to insufficient cycle life and low Coulombic efficiency (CE) [7,8]. Furthermore, the dendritic Li may also pierce the diaphragm, triggering internal short circuit in the battery, causing serious safety problem.

In order to solve the issue of dendritic Li growth, many strategies have been explored. For example, the growth of dendrites could be suppressed by preparing a solid electrolyte with high mechanical strength [8–10]. However, the low conductivity at room temperature and the large interfacial impedance seem to be difficult in application of solid electrolytes. Another strategy is to optimizing the electrolytes by producing a SEI film to inhibit the growth of dendrites, but this SEI is found to be continuously consumed during the charge/discharge cycling [11–13]. Although these methods could retard the growth of dendrites, they are not the solutions to inhibit the intrinsic nucleation growth of Li. Recently, the design or improvement of current collectors for anodes have attracted particular interests due to their regulation of lithium nucleation during the initial deposition process, which could determine the morphology of the subsequent lithium deposition [14–17]. For example, the preparation of a freestanding three-dimensional (3D) current collector, such as 3D porous Cu [18], nickel foam [19], carbon

* Corresponding author.
** Corresponding author. School of Environmental and Chemical Engineering, Shanghai University, Shanghai, 200444, China.
E-mail addresses: bzhao@shu.edu.cn (B. Zhao), jiujun.zhang@i.shu.edu.cn (J. Zhang).

https://doi.org/10.1016/j.nanoen.2020.104504
Received 1 December 2019; Received in revised form 8 January 2020; Accepted 14 January 2020
Available online 20 January 2020

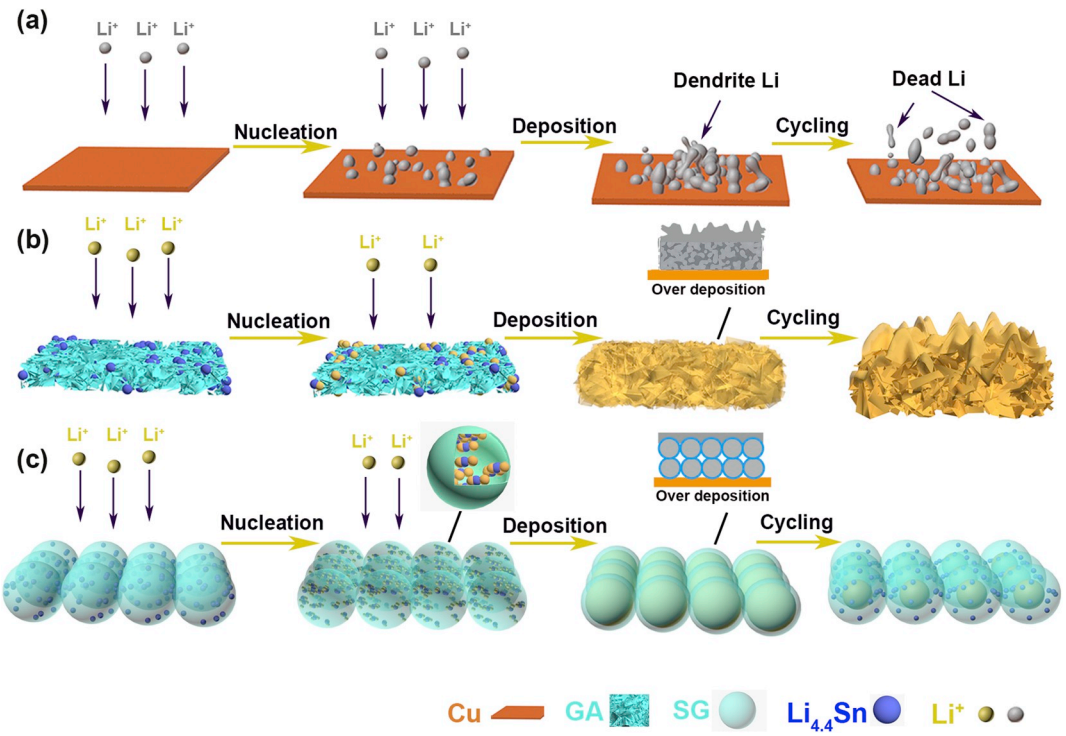

Fig. 1. Schematic illustration of the Li deposition processes on (a) bare Cu foil, (b) $Li_{4.4}Sn$/graphene aerogel, and (c) $Li_{4.4}Sn$/graphene hollow sphere electrodes. Li selectively nucleates and grows inside the hollow graphene spheres owing to the lithiophilic $Li_{4.4}Sn$ seeds, and then deposits at the surfaces of the graphene spheres at over deposition, leading to a small volumetric change and no dendrites out of the electrode.

fiber cloth [20–22], etc., which could reduce the growth of Li dendrites to some extent by reducing the local current density [23,24]. However, these freestanding 3D current collectors tend to be thicker, and the stored Li is often far overdone. Another method is to coat 3D conductive materials, such as graphene frame [14,17], carbon nanoflake [25], porous carbon [26], crumpled graphene [24], zeolitic imidazolate framework (ZIF) [27], etc., onto the current collector as the skeletons for Li deposition. The voids of these 3D porous materials can provide space for Li storage. However, the deposition of Li in the 3D materials usually tends to be anisotropic, resulting in a large amount of SEI is coated on the surface of the Li metal simultaneously. Therefore, the deposited Li cannot be combined in different directions [17], leading to low surface capacity.

In addition, as shown in Fig. 1a and b, there are a large number of tips in bare Cu foil and those 3D conductive scaffolds. The surface area decreases as the deposition amount increases, and the tip effect may appear gradually to produce Li dendrites on the electrode. To further explore the strategy for illuminating the dendrite growth of Li, Zheng et al. [28] coated a single layer of hollow carbon spheres on a Cu current collector as artificial SEI to guide the deposition of Li into a column. Whereas, the hollow carbon spheres could constantly move due to the weak binding with Cu substrate, and no Li storage contribution could be observed in this thin carbon film (~10 μm). Yan et al. [10] further introduced Au nanoparticles as the deposition seeds into the carbon spheres, demonstrating that Li preferentially nucleates on Au with low overpotential, which could guiding the deposition of Li inside the hollow carbon spheres. Their discovery and understanding of Li metal nucleation dependency opens up opportunities for space-controlled deposition. Tao et al. [29] synthesized ZnO quantum dots decorated hierarchical porous carbon as a framework for Li storage. Li deposition could be induced in the porous carbon by preformed highly conductive Li–Zn alloy. Zhang et al. [4] pre-plated a very thin tin layer on Cu foil, allowing the Li metal to first react with the Sn metal to form a Li–Sn alloy, which could guide the uniform deposition of Li on the Li–Sn alloy substrate.

The challenge is that the lithiophilic seeds were invariably decorated on the outer surfaces of the porous scaffolds (Fig. 1b) by additional processes, and their nonuniformity and intrinsic self-agglomeration properties might induce the unevenness of nucleation sites and undesirable formation and growth of Li dendrite.

In this work, we use non-tip and the interconnected hollow graphene spheres as the Li metal deposition container with internally loaded SnO_2 nanoparticles, which serve as the sources of lithiophilic $Li_{4.4}Sn$ seeds to guide uniform Li deposition inside the closed graphene spheres with high-areal-capacity (6 mA h cm^{-2}). The $Li_{4.4}Sn$ alloy has a low nucleation overpotential, and the simultaneously formed Li_2O owns excellent Li^+ ion conductive property [30]. As shown in Fig. 1c, Li metal can be preferentially deposited inside the hollow graphene spheres. This spherical Li can effectively avoid the growth of dendrites, and the closed encapsulation of graphene can significantly reduce the formation of SEI. Even when the hollow graphene spheres are completely filled with Li under overdeposition, Li can still be deposited on the surfaces of the graphene spheres. Since the connected spherical graphene can form a curved surface without a tip, the electronic field strength will be homogeneously dispersed. Therefore, Li metal can be uniformly deposited in the SnO_2/hollow graphene sphere (SnO_2/SG) scaffolds without generating dendrite, thereby leading to stable cycle performance and high cyclic Coulombic efficiency (CE). Specifically, it is observed that the SnO_2/SG electrode can be stable for at least 300 cycles at the current densities ranged from 0.5 to 5 mA cm^{-2}. An exceptionally low deposition overpotential of 18 mV (0.5 mA cm^{-2}, >1000 h) and high CE of 97.5% (over 150 cycles) are achieved.

2. Results and discussion

2.1. Fabrication and characterization of the SnO_2/SG

Graphene hollow sphere loaded nanosized tin oxide particles (SnO_2/SG) was synthesized by electrostatic self-wrapping of graphene oxide nanosheets and positively charged polystyrene/SnO_2 nanospheres and

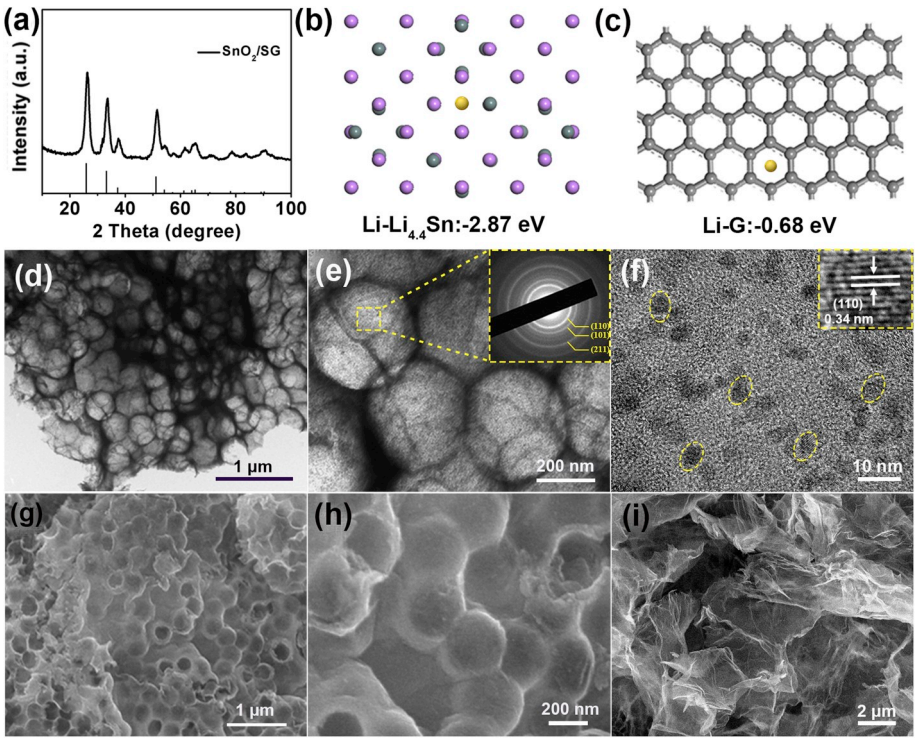

Fig. 2. (a) XRD pattern of the SnO_2/hollow graphene sphere scaffolds (SnO_2/SG). The optimized geometrical structures and corresponding binding energies (Eb) of a Li atom adsorbed on (b)$Li_{4.4}Sn$ and (c) graphene. Purple: Li in $Li_{4.4}Sn$; green: Sn; yellow: Li; gray: Carbon. (d, e) TEM, f) HRTEM and (g, h) SEM images of SnO_2/SG, presenting that the nucleation nano-seeds are uniformly dispersed within the hollow graphene spheres. (i) SEM image of SnO_2/graphene aerogel.

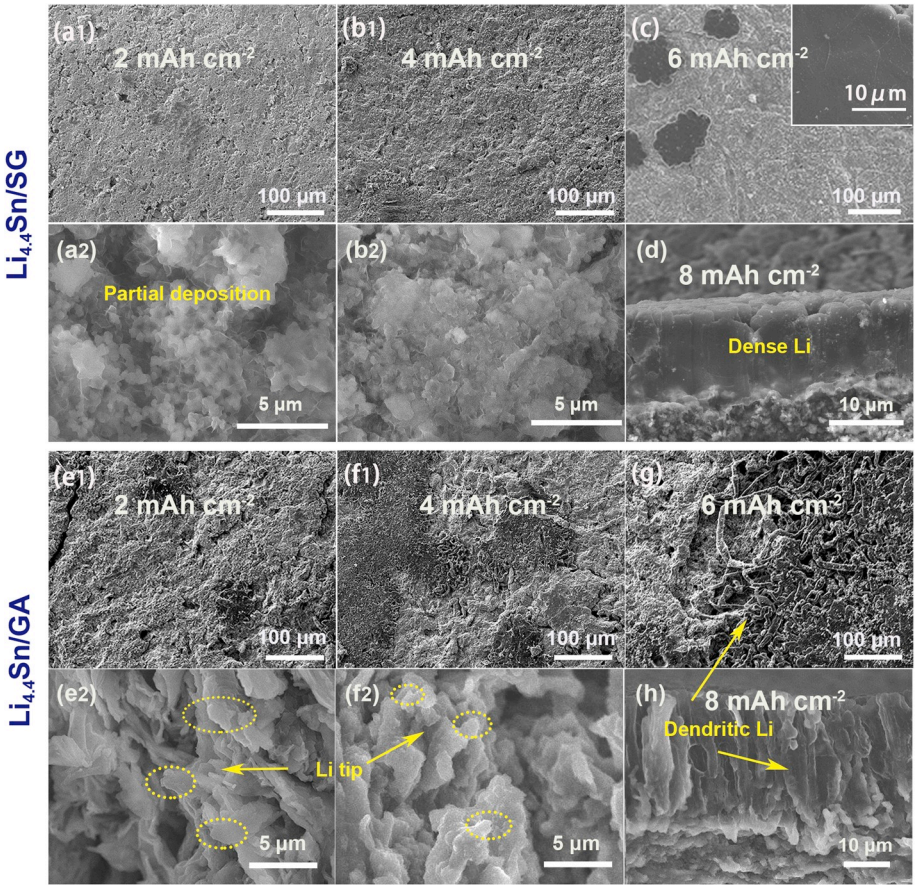

Fig. 3. SEM images of the $Li_{4.4}Sn$/SG (a–d) and $Li_{4.4}Sn$/GA (e–h) after plating at (a, e) 2 mA h cm^{-2}, (b, f) 4 mA h cm^{-2}, (c, g) 6 mA h cm^{-2}, and (d, h) 8 mA h cm^{-2} of Li into the electrodes, respectively. Note that Li is preferentially deposited inside the hollow graphene spheres; a smooth surface is presented even when the $Li_{4.4}Sn$/SG is completely deposited. In contrast, the tip effect would cause preferential Li deposition on the hump of graphene sheets, forming a flaky Li tips and mossy Li dendrites eventually on $Li_{4.4}Sn$/GA electrode.

followed by heat treatment as described in our previous work [31]. XRD (Fig. 2a) shows the diffraction peaks of SnO_2/SG, all of which are consistent with the orthorhombic SnO_2 (JPCDS No. 41–1445). Fig. 2d and g are the TEM and SEM images of SnO_2/SG showing the formation of an interconnected hollow graphene sphere structure with a diameter of about 300 nm. This structure can provide enough space for Li storage. Fig. 2e and f show that about 3 nm of SnO_2 nanoparticles are uniformly dispersed in the graphene hollow spheres. The diffraction ring corresponds to the (110), (101) and (211) crystal planes of SnO_2. The nano-SnO_2 particles can transform into nano-$Li_{4.4}Sn$ after Li ions intercalation, which is believed to have a remarkable affinity with Li. For fundamental understanding, DFT calculations were carried out to study the nucleation behavior of Li on $Li_{4.4}Sn$ and graphene. The $Li_{4.4}Sn$ has a large binding energy of −2.87 eV with Li (Fig. 2b), suggesting a strong interaction between Li and $Li_{4.4}Sn$. The binding energies of graphene to Li atoms at three different positions were also calculated, as shown in Fig. S1. The maximum binding energy (Fig. 2c) is only −0.68 eV, which is smaller than that of $Li_{4.4}Sn$ with Li. Thus $Li_{4.4}Sn$ will guide Li to preferentially nucleate and deposit inside the graphene sphere. For comparison, SnO_2/graphene aerogel (SnO_2/GA) with nanoparticle seeds decorated on the outer surface of graphene sheets was also synthesized, as shown in Fig. 2i. It can be seen that the aerogel shows a typical 3D open pore structure. The micro-sized voids can also provide space for the deposition of Li. In addition, the edges of graphene can form many tips during their linkage, which will collect a certain number of electrons. The magnified SEM images of these two electrodes deposited on the surface of the copper sheets show that the surface of SnO_2/SG (Fig. S2b) has a connected spherical shape with a highly uniform top surface without any distinct tip; while the surface of SnO_2/GA (Fig. S2d) has many tips formed by the corrugated graphene sheets.

2.2. Li metal deposition behavior

In order to explore the growth behavior of Li with samples SnO_2/SG, SnO_2/GA and bare Cu substrate, the morphologies of the three electrodes at different deposition capacities after discharged to 0 V were analyzed by SEM. The electrodes need to be pre-cycled before deposition, and SnO_2 can transform into $Li_{4.4}Sn$ after the pre-lithiation. Therefore, the pre-lithiated SnO_2/SG and SnO_2/GA as $Li_{4.4}Sn$/SG and $Li_{4.4}Sn$/GA were obtained, respectively. Fig. 3a–c shows the top view SEM images of the $Li_{4.4}Sn$/SG electrode with different Li deposition amounts. When the deposition capacities are 2 and 4 mA h cm^{-2}, metal Li does not appear on the surface of the electrode, indicating that Li is deposited inside the electrode material. Further enlargement shows that Li is preferentially deposited inside the graphene hollow sphere, which confirms our design, suggesting that the $Li_{4.4}Sn$ alloy formed at pre-cycling can successfully guide the preferential deposition of Li in the graphene sphere. At a deposition capacity of 2 mA h cm^{-2}, there are still many voids inside the sphere (Fig. 3a). Li metal is not completely filled with graphene sphere. When the deposition amount reaches to 4 mA h cm^{-2} (Fig. 3b), the voids inside the sphere are almost completely filled, the free volume and voids between the spheres are significantly reduced. A large amount of spherical Li surrounded by graphene shells can be observed. The spherical Li can effectively prevent Li from developing into dendrites, and the encapsulation of graphene can also reduce the formation of SEI film, thereby ensuring high Columbic efficiency (CE).

It is expected that the interior SnO_2 nanoseeds should be able to eliminate the nucleation barrier and guide the homogeneous Li deposition. To verify this, pure graphene hollow spheres (SGs) without any load are also designed, as shown in Fig. S3a and Fig. S3b. The SGs show a distinctly higher nucleation overpotential (~25 mV) than $Li_{4.4}Sn$/SG, as shown in Fig. S4a, presenting the depressed Li nucleation overpotential after the incorporation of lithiophilic $Li_{4.4}Sn$ phase. After deposition at 2 mA h cm^{-2}, a large amount of metallic Li can be observed on the surface of SG electrode (Fig. S3c). As can be seen from a further enlarged view (Fig. S3d and Fig. S3e), Li is deposited along the surface of the graphene sphere so that the morphology of the graphene sphere cannot be clearly observed. Thus, the Li metal is completely exposed to the electrolyte and the SEI is easily formed, resulting in low CE, which can only be stably maintained at around 92% for 70 cycles (Fig. S4b). Therefore, the short cycle life (~150 h) of the SG electrode is seen. For the $Li_{4.4}Sn$/GA electrode (Fig. 3e–h), some Li metal can be observed on the surface of the electrode material with deposition amounts of 2 and 4 mA h cm^{-2}. From the enlarged view of Fig. 3e2, it can be seen that the deposition of Li in the graphene aerogel starts from the surface of the graphene and forms a Li sheet rather than filling the pores of the electrode. This probably because of the planar distribution of tin seeds and the tip effect of the disordered stacked graphene sheets [32]. Especially, the tip effect would further cause preferential Li deposition on the hump and form a large number of flaky lithium tips (as marked by the yellow-dashed circles), which will could a potential risk of the growth of dendritic Li on one hand, and on the other, they are completely exposed to the electrolyte, which will continuously produce a SEI film on the fresh interface and reduce the CE.

When the deposition amount reaches to 6 mA h cm^{-2}, it is observed that the voids inside and between the graphene spheres are completely filled with $Li_{4.4}Sn$/SG, resulting in a smooth surface (Fig. 3c). This value is generally consistent with the volume of pores left by the decomposition of the added polystyrene sphere templates (the specific calculation process is shown in Supporting Information). According to the mass ratio of the added polystyrene spheres, the volume are totally filled by active Li (with a theoretical capacity of 3860 mA h g^{-1}), which can be estimated by that the Li spheres of the pole piece can hold an aerial capacity of 6.23 mA h cm^{-2}. The slightly lower value might be attributed to the three factors, such as the intrinsic volume of SnO_2 nucleation nano-seeds, the incomplete wrapping of graphene on PS and the slight structure collapse of the hollow spheres during calcination. Therefore, Li is preferentially plated inside the hollow graphene spheres with a negligible thickness increase of the electrode even at a high deposition amount of 6 mA h cm^{-2} (Figs. S5a–d). Further Li deposition takes place at the surfaces of the graphene spheres after the void space is fully filled, exhibiting a uniform surface (as shown in the inset of Fig. 3c), which is distinctly different from the dendritic Li on the GA surface (Fig. 3e–h). When over-deposited to 8 mA h cm^{-2}, a layer of Li metal of about 10 μm is deposited on the surface of $Li_{4.4}Sn$/SG (Fig. 3d and Fig. S5e from the cross-sections), agreeing with the theoretical capacity of the increased Li loading. This Li metal layer is very dense and uniform, which confirms our design that the hollow sphere structure allows the electrode to form a curved, tipless surface, effectively suppressing the formation of Li dendrite and ensuring uniform deposition of Li metal. In addition, the 3D interconnected structure of the spherical graphene remains well preserved after totally stripping the plated 6 mA h cm^{-2} of Li (Fig. S5f). The scalable Li loading with tolerable volume fluctuation demonstrates the excellent structural integrity of such a hollow $Li_{4.4}Sn$/SG electrode.

However, on the surface of $Li_{4.4}Sn$/GA electrode (Fig. 3h), a thick layer of ~17 μm Li metal is formed at 8 mA h cm^{-2}, consisting of the countless erect dendrites, which cannot be combined due to the encapsulation of the SEI. The diameter of the dendritic Li is about 2 μm, which is similar in size to the Li bumps at the tip of graphene sheets for the electrode depositing 4 mA h cm^{-2} (Fig. 3f2). Therefore, it can be inferred that the dendritic Li is grown from the Li on the tip of conductive skeleton with the scattered graphene at a large deposition amount. For the bare Cu substrate, a large amount of Li dendrites can be found on the surface at the varied deposition capacities of 2–6 mA h cm^{-2} (Fig. S6). This is reason why the $Li_{4.4}Sn$/SG and Cu electrodes fail quickly.

2.3. Electrochemical performance

Metal Li-based anodes typically have low CE and short cycle life, which limit their practical application. To determine whether the graphene hollow sphere structure can improve the Li deposition

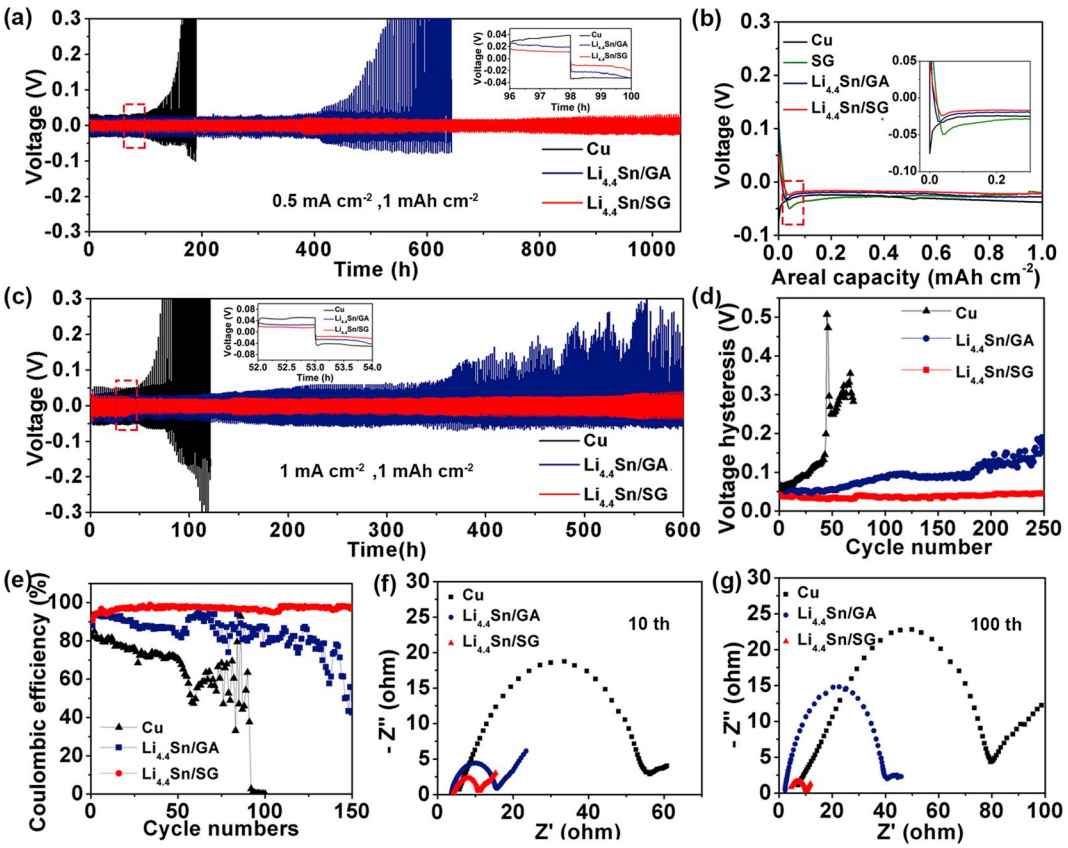

Fig. 4. Voltage–time profiles of the $Li_{4.4}Sn$/SG, $Li_{4.4}Sn$/GA and Cu electrodes at (a) 0.5 and (c) 1 mA cm^{-2} with a limited capacity of 1 mA h cm^{-2}; (b) voltage profiles of Li plating/stripping; (d) voltage hysteresis variation with cycling number; (e) Coulombic efficiencies at 1 mA cm^{-2} with a capacity limited to 2 mA h cm^{-2}. (f) and (g) Nyquist plots of Cu, $Li_{4.4}Sn$/GA, and $Li_{4.4}Sn$/SG cells at the 10th and 100th cycles, respectively.

performance, SnO_2/SG, SnO_2/GA and Cu anodes were assembled into coin cells with Li and cycled at the current densities of 0.5, 1, 2, 3 and 5 mA cm^{-2}, respectively. Before galvanostatic cycling, 8 mA h cm^{-2} of Li was pre-plated onto electrodes to form $Li_{4.4}Sn$/SG, $Li_{4.4}Sn$/GA and Cu electrodes, respectively. Fig. 4a shows the voltage profiles of the three cells with for 1 mA h cm^{-2} at 0.5 mA cm^{-2}. It can be clearly seen that the $Li_{4.4}Sn$/SG anode not only exhibits a low deposition overpotential (~18 mV), but also achieves excellent cycle stability for more than 1000 h (~300 cycles), which means the stable Li plating/stripping processes forming a stable Li/electrolyte interface. However, the $Li_{4.4}Sn$/GA and Cu electrodes show larger deposition overpotential and rapid rise in voltage, which could be attributed to the formation of dead Li as a result of uneven deposition, resulting in the pre-stored Li being quickly consumed. When the current density is increased to 1 mA cm^{-2} (Fig. 4c), $Li_{4.4}Sn$/GA and Cu electrodes show higher overpotential and earlier voltage rise. $Li_{4.4}Sn$/GA electrode experiences severe voltage oscillations after 175 cycles, which means that uneven Li deposition can lead to an unstable Li/electrolyte interface. The $Li_{4.4}Sn$/SG electrode still shows a moderate overpotential of 34 mV after 600 h (300 cycles). The $Li_{4.4}Sn$/SG electrode can also be stably cycled over 300 cycles at large current densities of 2 mA cm^{-2}, 3 mA cm^{-2} and even 5 mA cm^{-2} (Fig. S7). Even when the capacity or current density is increased (Figs. S8a and b), $Li_{4.4}Sn$/SG still shows the best cycle performance (stably cycling for 200 h).

Fig. 4b shows the voltage distribution of Li plating/stripping in three samples. As reported, the voltage dip on the plating curve is caused by the nucleation barrier [10,33]. From Fig. 4b, it can be seen that $Li_{4.4}Sn$/SG and $Li_{4.4}Sn$/GA have only a low nucleation overpotential of 8 mV compared to that of SG (25 mV) and bare Cu (50 mV) due to the formation of highly lithophilic $Li_{4.4}Sn$ and the reduced local current density by 3D conductive framework [4]. Fig. 4d provides the voltage hysteresis curves upon cycling. It is shown that the voltage hysteresis of $Li_{4.4}Sn$/SG can be stably maintained at 38 mV in 250 cycles, whereas that of $Li_{4.4}Sn$/GA and Cu continues to increase, indicating that more driving force is required to maintain this current density of 0.5 mA cm^{-2}. The main reason is that the dead Li formed by Li dendrite breaks and continuously forms SEI after many cycles. The sudden voltage drop of the Cu foil battery in the figure is mainly due to the micro short circuit caused by the growth of dendrites.

To further investigate the cyclic stability of these three electrodes, Coulombic efficiencies were evaluated under different current densities and deposition area capacities. Fig. 4e shows that at a current density of 0.5 mA cm^{-2} with a limited capacity of 1 mA h cm^{-2}, the $Li_{4.4}Sn$/SG electrode can maintain a CE of about 97.5% after 150 cycles, while the initial Coulomb efficiencies of $Li_{4.4}Sn$/GA and Cu electrodes are only 90% and 82%, respectively, and decreased rapidly after 90 and 50 cycles. When the capacity or current density increases (Figs. S9a and b), $Li_{4.4}Sn$/SG still exhibits the highest and the most stable CE, while those of two control electrodes are rapidly reduced and present large fluctuations. The decrease in CE can be mainly attributed to the formation of dendrites in $Li_{4.4}Sn$/GA and Cu electrodes during the deposition process, which can enlarge the contact of the freshly exposed Li with the electrolyte, thereby increase the formation of the SEI film, causing Li to lose electrical contact and become dead Li, thereby greatly reduce the CE. Fig. S10 and Fig. S11 show the voltage curves of the three electrodes at different current densities and deposition area capacities. It can be found that the Li deposition and dissolution curves of $Li_{4.4}Sn$/SG electrode hardly change after 150 cycles, indicating that the deposition and stripping processes of Li is very stable without SET thickening SEI and the formation of dead Li. For $Li_{4.4}Sn$/GA and Cu electrodes, not only the amount of Li removal is decreasing, but also the deposition potential is increasing, indicating that the amount of dead Li is increasing and the

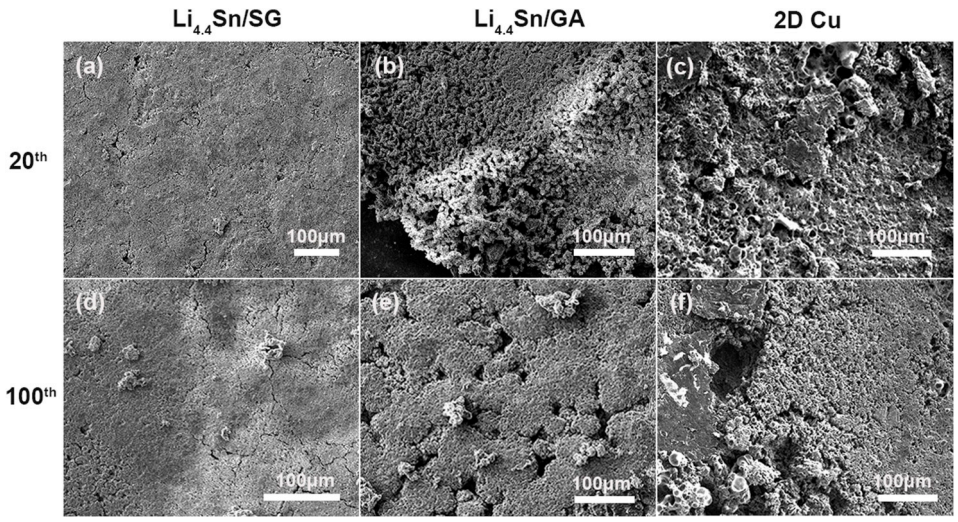

Fig. 5. Top-view SEM images of (a, d) $Li_{4.4}Sn$/SG, (b, e) $Li_{4.4}Sn$/GA and (c, f) Cu electrodes after 20 cycles and 100 cycles at 2 mA cm^{-2}. $Li_{4.4}Sn$/SG presents the flat and dendrite-free surfaces upon cycling; whereas a larger amount of dead Li with thick SEI are observed in $Li_{4.4}Sn$/GA and bare Cu electrodes.

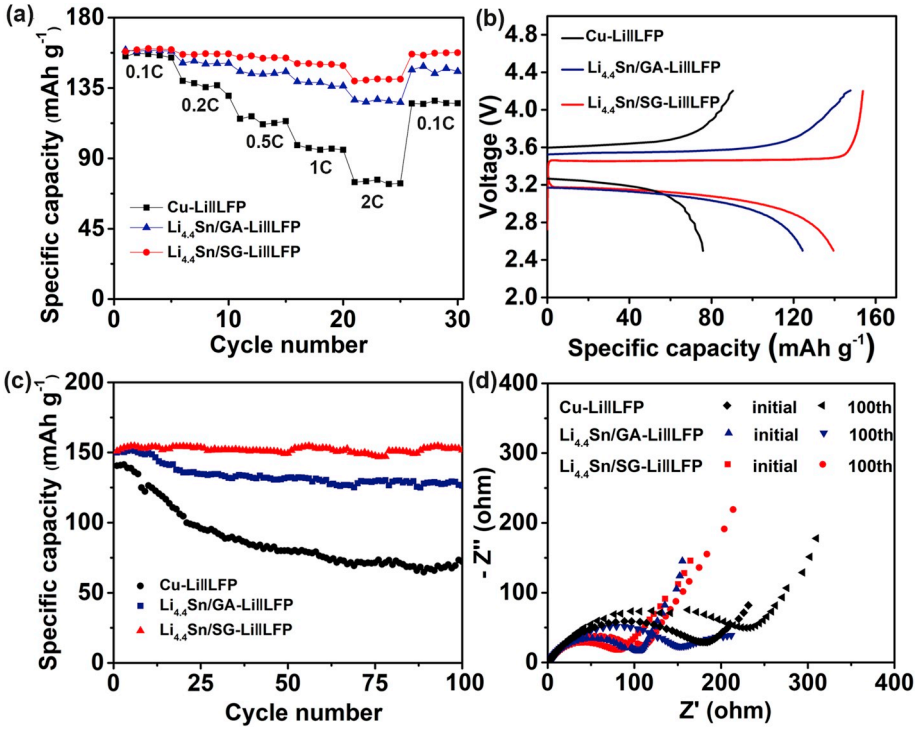

Fig. 6. (a) Rate capability under various rates from 0.1C to 2C. (b) Corresponding charge/discharge curves of the full cells at 2C. (c) Cycling performance of the Cu–Li||LFP, $Li_{4.4}Sn$/GA-Li||LFP and $Li_{4.4}Sn$/SG-Li||LFP full cells at 1C (d) Nyquist plots of Cu–Li||LFP, $Li_{4.4}Sn$/GA-Li||LFP and $Li_{4.4}Sn$/SG-Li||LFP full cells at the initial and 100th cycles.

SEI is continuously thickening. The results are consistent with the Nyquist plots of the three electrodes after 10th and 100th cycles (Fig. 4f and g). The semicircle diameters of $Li_{4.4}Sn$/GA and Cu electrodes are increased from 16 to 54 Ω in the 10th cycle to 40 and 80 Ω in the 100th cycle, respectively, which indicates the thickening of the SEI. In contrast, thinner and much stable SEI is found in $Li_{4.4}Sn$/SG because it has a lower and almost unchanged semicircle diameter. Above mentioned SEM observations (Fig. 3) also show that the uniform Li deposition behavior makes it easier to keep SEI stable. $Li_{4.4}Sn$/GA and Cu electrodes continue to consume Li ions and build SEI, resulting in a high resistance film and low CE. Eventually, the dendrites pierce the separator and cause a short circuit in the battery. The results of $Li_{4.4}Sn$/SG electrode can demonstrate that such an electrode can have high cycle stability compared to $Li_{4.4}Sn$/GA and Cu electrodes.

In order to better understand the deposition and stripping behavior of Li during cycling, top-view SEM images of the three electrodes after different cycles were recorded. Fig. 5a and Fig. 5d show that the surface of $Li_{4.4}Sn$/SG is very flat after 20 and 100 cycles without the formation of dendritic Li or dead Li. However, there are many dendrites, pits, gaps and dead Li on the surface of $Li_{4.4}Sn$/GA, and at the same time, there is a larger amount of dead Li with thick SEI on the surface of bare Cu substrate. The generation of dendrites and dead Li can significantly decrease the CE of the electrode, which is also responsible for the high deposition overpotentials of $Li_{4.4}Sn$/GA and Cu. The main reason for this is that the

local current density is not uniform during the initial deposition, resulting in non-uniform nucleation of Li on the $Li_{4.4}Sn$/GA and Cu material surfaces, leading to the formation of dendrite in the subsequent cycles. The growth of Li then continues along the already grown dendrites until the break and the formation of the dead Li. The 3D hollow sphere structure of $Li_{4.4}Sn$/SG can not only encapsulate Li in the sphere to avoid the generation of dendrites, but also provide a tipless surface to reduce the local current density, thereby guiding the uniform deposition of Li.

In order to validate the feasibility of $Li_{4.4}Sn$/SG-Li anode for the application of practical battery system, commercial $LiFePO_4$ (LFP) cathode with a high surface load of 12 mg cm^{-2} (2.0 mA h cm^{-2}) was paired with Cu–Li, $Li_{4.4}Sn$/GA-Li, and $Li_{4.4}Sn$/SG-Li anodes to assemble full cells. It can be seen that $Li_{4.4}Sn$/GA-Li‖LFP shows the best rate performance (Fig. 6a) due to the low resistance caused by uniformly deposited Li. Even at 2C, $Li_{4.4}Sn$/SG-Li‖LFP still has a discharge capacity of about 140 mA h g^{-1}. In addition, $Li_{4.4}Sn$/SG-Li‖LFP also shows the smallest charging polarization (Fig. 6b), which corresponds to the lower lithium deposition overpotential of the $Li_{4.4}Sn$/SG-Li electrode (Fig. S7). Fig. 6c illustrates the cycle stability at 1.0C. $Li_{4.4}Sn$/SG-Li‖LFP full cells can be cycled for more than 100 cycles with a capacity of 150 mA h g^{-1}, while the capacity of $Li_{4.4}Sn$/GA-Li‖LFP and Cu–Li‖LFP begins to decay at 15 cycles due to the formation of large amounts of dead Li, which corresponds to their uneven Li deposition behavior. Therefore, the impedance of $Li_{4.4}Sn$/GA-Li‖LFP and Cu–Li‖LFP increases significantly after 100 cycles, while the impedance of $Li_{4.4}Sn$/SG-Li‖LFP is almost unchanged, which is all due to the uniform lithium deposition of the $Li_{4.4}Sn$/SG-Li electrode.

3. Conclusion

In summary, we have successfully fabricated a closed three-dimensional hollow graphene sphere with an internal load of $Li_{4.4}Sn$ nanoparticles ($Li_{4.4}Sn$/SG), obtained by Li intercalation of nano-SnO_2, for stable Li metal anodes without dendrite. Such $Li_{4.4}Sn$ nanoparticles are uniformly encapsulated inside the graphene spheres. Both DFT calculations and experimental studies have shown that $Li_{4.4}Sn$ has a higher binding energy for Li and a lower nucleation overpotential for Li than graphene. Therefore, it can induce the nucleation and growth processes of Li occurring in the hollow spheres to avoid the growth of Li dendrite and reduce the formation of SEI. Moreover, even after the hollow spheres are filled with Li metal, Li can still deposit on the surfaces of the graphene spheres to obtain a dense Li metal layer free of dendrite due to that the connected and smooth spherical surface can intrinsically repel tip effect. In this way, the obtained $Li_{4.4}Sn$/SG-Li anode exhibits a long cycle life of more than 1000 h (300 cycles) and a high CE (97.5% retention after 150 cycles). We believe that the design of this closed hollow spherical structure with lithiophilic nanoparticle seeds inside is a promising strategy to accommodate Li, and can provide an inspiration to the design principles for Li metal anodes.

Declaration of competing interest

The authors declare that they have no known competing financial interests or personal relationships that could have appeared to influence the work reported in this paper.

Acknowledgements

The authors acknowledge funding support from the National Natural Science Foundation of China (11575105, 21501119 and 21671130).

Appendix A. Supplementary data

Supplementary data to this article can be found online at https://doi.org/10.1016/j.nanoen.2020.104504.

References

[1] H. Kim, G. Jeong, Y.U. Kim, J.H. Kim, C.M. Park, H.J. Sohn, Chem. Soc. Rev. 42 (2013) 9011–9034.
[2] T. Li, X.-Z. Yuan, L. Zhang, D. Song, K. Shi, C. Bock, Electrochem. Energy Rev. 2 (2019) 1–38.
[3] X.B. Cheng, H.J. Peng, J.Q. Huang, R. Zhang, C.Z. Zhao, Q. Zhang, ACS Nano 9 (2015) 6373–6382.
[4] S.S. Zhang, X. Fan, C. Wang, Electrochim. Acta 258 (2017) 1201–1207.
[5] W. Xu, J. Wang, F. Ding, X. Chen, E. Nasybulin, Y. Zhang, J.-G. Zhang, Energy Environ. Sci. 7 (2014) 513–537.
[6] H. Wang, Y. Liu, Y. Li, Y. Cui, Electrochem. Energy Rev. 2 (2019) 509–517.
[7] X.B. Cheng, R. Zhang, C.Z. Zhao, Q. Zhang, Chem. Rev. 117 (2017) 10403–10473.
[8] E. Umeshbabu, B. Zheng, Y. Yang, Electrochem. Energy Rev. 2 (2019) 199–230.
[9] X.B. Cheng, R. Zhang, C.Z. Zhao, F. Wei, J.G. Zhang, Q. Zhang, Adv. Sci. 3 (2016) 1500213.
[10] N.W. Li, Y.X. Yin, C.P. Yang, Y.G. Guo, Adv. Mater. 28 (2016) 1853–1858.
[11] F. Ding, W. Xu, G.L. Graff, J. Zhang, M.L. Sushko, X. Chen, Y. Shao, M. H. Engelhard, Z. Nie, J. Xiao, X. Liu, P.V. Sushko, J. Liu, J.G. Zhang, J. Am. Chem. Soc. 135 (2013) 4450–4456.
[12] W. Li, H. Yao, K. Yan, G. Zheng, Z. Liang, Y.M. Chiang, Y. Cui, Nat. Commun. 6 (2015), 7436-7354.
[13] Y. Lu, S.K. Das, S.S. Moganty, L.A. Archer, Adv. Mater. 24 (2012) 4430–4435.
[14] J. Pu, J. Li, Z. Shen, C. Zhong, J. Liu, H. Ma, J. Zhu, H. Zhang, P.V. Braun, Adv. Funct. Mater. 28 (2018) 1804133.
[15] J. Guo, S. Zhao, H. Yang, F. Zhang, J. Liu, J. Mater. Chem. A 7 (2019) 2184–2191.
[16] F. Liang, L. Lin, Z. Feng, C. Chu, J. Pan, J. Yang, Y. Qian, J. Mater. Chem. A 7 (2019) 8765–8770.
[17] R. Zhang, X.R. Chen, X. Chen, X.B. Cheng, X.Q. Zhang, C. Yan, Q. Zhang, Angew. Chem., Int. Ed. Engl. 56 (2017) 7764–7768.
[18] Q. Li, S. Zhu, Y. Lu, Adv. Funct. Mater. 27 (2017) 1606422.
[19] S.-S. Chi, Y. Liu, W.-L. Song, L.-Z. Fan, Q. Zhang, Adv. Funct. Mater. 27 (2017) 1700348.
[20] S. Wu, Z. Zhang, M. Lan, S. Yang, J. Cheng, J. Cai, J. Shen, Y. Zhu, K. Zhang, W. Zhang, Adv. Mater. 30 (2018) 1705830.
[21] R. Zhang, X. Chen, X. Shen, X.-Q. Zhang, X.-R. Chen, X.-B. Cheng, C. Yan, C.-Z. Zhao, Q. Zhang, Joule 2 (2018) 764–777.
[22] X. Ji, D.-Y. Liu, D.G. Prendiville, Y. Zhang, X. Liu, G.D. Stucky, Nano Today 7 (2012) 10–20.
[23] K. Yan, B. Sun, P. Munroe, G. Wang, Energy Storage Mater. 11 (2018) 127–133.
[24] S. Liu, A. Wang, Q. Li, J. Wu, K. Chiou, J. Huang, J. Luo, Joule 2 (2018) 184–193.
[25] Q. Sun, W. Zhai, G. Hou, J. Feng, L. Zhang, P. Si, S. Guo, L. Ci, ACS Sustain. Chem. Eng. 6 (2018) 15219–15227.
[26] T. Wang, R. Villegas Salvatierra, A.S. Jalilov, J. Tian, J.M. Tour, ACS Nano 11 (2017) 10761–10767.
[27] L. Wang, X. Zhu, Y. Guan, J. Zhang, F. Ai, W. Zhang, Y. Xiang, S. Vijayan, G. Li, Y. Huang, G. Cao, Y. Yang, H. Zhang, Energy Storage Mater. 11 (2018) 191–196.
[28] G. Zheng, S.W. Lee, Z. Liang, H.W. Lee, K. Yan, H. Yao, H. Wang, W. Li, S. Chu, Y. Cui, Nat. Nanotechnol. 9 (2014) 618–623.
[29] L. Liu, Y.-X. Yin, J.-Y. Li, N.-W. Li, X.-X. Zeng, H. Ye, Y.-G. Guo, L.-J. Wan, Joule 1 (2017) 563–575.
[30] Y. Liu, S. Zhang, X. Qin, F. Kang, G. Chen, B. Li, Nano Lett. 19 (2019) 4601–4607.
[31] B. Zhao, Z. Wang, F. Chen, Y. Yang, Y. Gao, L. Chen, Z. Jiao, L. Cheng, Y. Jiang, ACS Appl. Mater. Interfaces 9 (2017) 1407–1415.
[32] X. Shen, H. Liu, X.-B. Cheng, C. Yan, J.-Q. Huang, Energy Storage Mater. 12 (2018) 161–175.
[33] Z. Lu, Q. Liang, B. Wang, Y. Tao, Y. Zhao, W. Lv, D. Liu, C. Zhang, Z. Weng, J. Liang, H. Li, Q.-H. Yang, Adv. Energy Mater. 9 (2019) 1803186.

Yong Jiang received his Ph.D. degree from Shanghai University in 2013. He is currently an Associate Professor in School of Environmental and Chemical Engineering at Shanghai University. His research interests include Li-metal batteries, solid-state electrolytes, novel anode materials and their potential applications in energy storage and conversion.

Jinlong Jiang is currently a Master candidate in the School of Environmental and Chemical Engineering at the Shanghai University. His research interests include lithium metal batteries, solid-state electrolytes, all solid-state LIBs.

Zhixuan Wang is currently a Ph.D. candidate in the School of Environmental and Chemical Engineering at the Shanghai University, China. Currently, his research interests include lithium metal batteries, solid-state electrolytes, all solid-state LIBs and Li–S batteries, and the interfacial study in all-solid-state batteries.

Mingrui Han is currently a Master candidate in the School of Environmental and Chemical Engineering at the Shanghai University. His main research interest is in structural design for lithium/sodium metal anode.

Xiaoyu Liu received her Ph.D. degree in Physical Chemistry from Fudan University in 2016. She currently works in Shanghai University. Her research focuses on the design of novel functional materials and their applications in energy storage.

Jin Yi received his Ph.D. from Fudan University in 2014, and later worked as a postdoctoral researcher in National Institute of Advanced Industrial Science and Technology (AIST), Japan. He currently works in Shanghai University. His research interests involve electrochemical functional materials and their application in Li batteries, solid-state batteries and metal-air batteries.

Professor Bing Zhao obtained his Ph.D. from Institute of Solid State Physics, Chinese Academy of Science, and later worked as a postdoctoral researcher in Tsinghua University. He is now a professor in School of Environmental and Chemical Engineering and Institute for Sustainable Energy at Shanghai University. His research focuses on designing and fabrication of novel functional nanostructured materials for energy storage. Potential applications range from energy storage devices and power systems such as lithium-ion batteries, lithium-sulfur batteries, solid-state batteries. He is honored to receive the 2013 Shanghai Excellent Technical Leader Project.

Professor Xueliang Sun is a Canada Research Chair in Development of Nanomaterials for Clean Energy, Fellow of the Royal Society of Canada and Canadian Academy of Engineering and Full Professor at the University of Western Ontario, Canada. Dr. Sun received his Ph.D. in materials chemistry in 1999 from the University of Manchester, UK, which he followed up by working as a postdoctoral fellow at the University of British Columbia, Canada and as a Research Associate at L′ Institut National de la Recherche Scientifique (INRS), Canada. His current research interests are focused on advanced materials for electrochemical energy storage and conversion.

Professor Jiujun Zhang is a Professor at Shanghai University, and former Principal Research Officer at the National Research Council of Canada Energy (NRC). Dr. Zhang received his BS and MSc in electrochemistry from Peking University in 1982 and 1985, respectively, and his PhD in electrochemistry from Wuhan University in 1988. He then carried out three terms of postdoctoral research at the California Institute of Technology, York University, and the University of British Columbia. Dr. Zhang has over 30 years of scientific research experience, particularly in the area of electrochemical energy storage and conversion.